DESY 00-142
October 2000

Measurement of dijet cross sections for events with a leading neutron in photoproduction at HERA

ZEUS Collaboration

Abstract

Differential cross sections for dijet photoproduction in association with a leading neutron using the reaction $e^+ + p \to e^+ + n + \text{jet} + \text{jet} + X_r$ have been measured with the ZEUS detector at HERA using an integrated luminosity of 6.4 pb^{-1}. The fraction of dijet events with a leading neutron in the final state was studied as a function of the jet kinematic variables. The cross sections were measured for jet transverse energies $E_{\rm T}^{\rm jet} > 6$ GeV, neutron energy $E_n > 400$ GeV, and neutron production angle $\theta_n < 0.8$ mrad. The data are broadly consistent with factorization of the lepton and hadron vertices and with a simple one-pion-exchange model.

The ZEUS Collaboration

J. Breitweg, S. Chekanov, M. Derrick, D. Krakauer, S. Magill, B. Musgrave, A. Pellegrino, J. Repond, R. Stanek, R. Yoshida
Argonne National Laboratory, Argonne, IL, USA [p]

M.C.K. Mattingly
Andrews University, Berrien Springs, MI, USA

P. Antonioli, G. Bari, M. Basile, L. Bellagamba, D. Boscherini[1], A. Bruni, G. Bruni, G. Cara Romeo, L. Cifarelli[2], F. Cindolo, A. Contin, M. Corradi, S. De Pasquale, P. Giusti, G. Iacobucci, G. Levi, A. Margotti, T. Massam, R. Nania, F. Palmonari, A. Pesci, G. Sartorelli, A. Zichichi
University and INFN Bologna, Bologna, Italy [f]

C. Amelung[3], A. Bornheim[4], I. Brock, K. Coböken[5], J. Crittenden[1], R. Deffner[6], H. Hartmann, K. Heinloth[7], E. Hilger, P. Irrgang, H.-P. Jakob, A. Kappes[8], U.F. Katz, R. Kerger, E. Paul, J. Rautenberg,
H. Schnurbusch, A. Stifutkin, J. Tandler, K.C. Voss, A. Weber, H. Wieber
Physikalisches Institut der Universität Bonn, Bonn, Germany [c]

D.S. Bailey, O. Barret, N.H. Brook[9], B. Foster[1], G.P. Heath, H.F. Heath, E. Rodrigues[10], J. Scott, R.J. Tapper
H.H. Wills Physics Laboratory, University of Bristol, Bristol, U.K. [o]

M. Capua, A. Mastroberardino, M. Schioppa, G. Susinno
Calabria University, Physics Dept.and INFN, Cosenza, Italy [f]

H.Y. Jeoung, J.Y. Kim, J.H. Lee, I.T. Lim, K.J. Ma, M.Y. Pac[11]
Chonnam National University, Kwangju, Korea [h]

A. Caldwell, W. Liu, X. Liu, B. Mellado, S. Paganis, S. Sampson, W.B. Schmidke, F. Sciulli
Columbia University, Nevis Labs., Irvington on Hudson, N.Y., USA [q]

J. Chwastowski, A. Eskreys, J. Figiel, K. Klimek, K. Olkiewicz, K. Piotrzkowski[3], M.B. Przybycień, P. Stopa, L. Zawiejski
Inst. of Nuclear Physics, Cracow, Poland [j]

B. Bednarek, K. Jeleń, D. Kisielewska, A.M. Kowal, T. Kowalski, M. Przybycień, E. Rulikowska-Zarębska, L. Suszycki, D. Szuba
Faculty of Physics and Nuclear Techniques, Academy of Mining and Metallurgy, Cracow, Poland [j]

A. Kotański
Jagellonian Univ., Dept. of Physics, Cracow, Poland [k]

L.A.T. Bauerdick, U. Behrens, J.K. Bienlein, K. Borras, V. Chiochia, D. Dannheim, K. Desler, G. Drews, A. Fox-Murphy, U. Fricke, F. Goebel, S. Goers, P. Göttlicher, R. Graciani, T. Haas, W. Hain, G.F. Hartner, K. Hebbel, S. Hillert, W. Koch[12]†, U. Kötz, H. Kowalski, H. Labes, B. Löhr, R. Mankel, J. Martens, M. Martínez, M. Milite, M. Moritz, D. Notz, M.C. Petrucci, A. Polini, M. Rohde[7], A.A. Savin, U. Schneekloth, F. Selonke, M. Sievers[13], S. Stonjek, G. Wolf, U. Wollmer, C. Youngman, W. Zeuner
Deutsches Elektronen-Synchrotron DESY, Hamburg, Germany

C. Coldewey, A. Lopez-Duran Viani, A. Meyer, S. Schlenstedt, P.B. Straub
DESY Zeuthen, Zeuthen, Germany

G. Barbagli, E. Gallo, A. Parenti, P. G. Pelfer
University and INFN, Florence, Italy [f]

A. Bamberger, A. Benen, N. Coppola, S. Eisenhardt[14], P. Markun, H. Raach, S. Wölfle
Fakultät für Physik der Universität Freiburg i.Br., Freiburg i.Br., Germany [c]

P.J. Bussey, M. Bell, A.T. Doyle, C. Glasman, S.W. Lee[15], A. Lupi, N. Macdonald, G.J. McCance, D.H. Saxon, L.E. Sinclair, I.O. Skillicorn, R. Waugh
Dept. of Physics and Astronomy, University of Glasgow, Glasgow, U.K. [o]

I. Bohnet, N. Gendner, U. Holm, A. Meyer-Larsen, H. Salehi, K. Wick
Hamburg University, I. Institute of Exp. Physics, Hamburg, Germany [c]

T. Carli, A. Garfagnini, I. Gialas[16], L.K. Gladilin[17], D. Kçira[18], R. Klanner, E. Lohrmann
Hamburg University, II. Institute of Exp. Physics, Hamburg, Germany [c]

R. Gonçalo[10], K.R. Long, D.B. Miller, A.D. Tapper, R. Walker
Imperial College London, High Energy Nuclear Physics Group, London, U.K. [o]

P. Cloth, D. Filges
Forschungszentrum Jülich, Institut für Kernphysik, Jülich, Germany

T. Ishii, M. Kuze, K. Nagano, K. Tokushuku[19], S. Yamada, Y. Yamazaki
Institute of Particle and Nuclear Studies, KEK, Tsukuba, Japan [g]

S.H. Ahn, S.B. Lee, S.K. Park
Korea University, Seoul, Korea [h]

H. Lim[15], D. Son
Kyungpook National University, Taegu, Korea [h]

F. Barreiro, G. García, O. González, L. Labarga, J. del Peso, I. Redondo[20], J. Terrón, M. Vázquez
Univer. Autónoma Madrid, Depto de Física Teórica, Madrid, Spain [n]

M. Barbi, F. Corriveau, D.S. Hanna, A. Ochs, S. Padhi, D.G. Stairs, M. Wing
McGill University, Dept. of Physics, Montréal, Québec, Canada [a], [b]

T. Tsurugai
Meiji Gakuin University, Faculty of General Education, Yokohama, Japan

A. Antonov, V. Bashkirov[21], M. Danilov, B.A. Dolgoshein, D. Gladkov, V. Sosnovtsev, S. Suchkov
Moscow Engineering Physics Institute, Moscow, Russia [l]

R.K. Dementiev, P.F. Ermolov, Yu.A. Golubkov, I.I. Katkov, L.A. Khein, N.A. Korotkova, I.A. Korzhavina, V.A. Kuzmin, O.Yu. Lukina, A.S. Proskuryakov, L.M. Shcheglova, A.N. Solomin, N.N. Vlasov, S.A. Zotkin
Moscow State University, Institute of Nuclear Physics, Moscow, Russia [m]

C. Bokel, M. Botje, N. Brümmer, J. Engelen, S. Grijpink, E. Koffeman, P. Kooijman, S. Schagen, A. van Sighem, E. Tassi, H. Tiecke, N. Tuning, J.J. Velthuis, J. Vossebeld, L. Wiggers, E. de Wolf
NIKHEF and University of Amsterdam, Amsterdam, Netherlands [i]

B. Bylsma, L.S. Durkin, J. Gilmore, C.M. Ginsburg, C.L. Kim, T.Y. Ling
Ohio State University, Physics Department, Columbus, Ohio, USA [p]

S. Boogert, A.M. Cooper-Sarkar, R.C.E. Devenish, J. Große-Knetter[22], T. Matsushita, O. Ruske,
M.R. Sutton, R. Walczak
Department of Physics, University of Oxford, Oxford U.K. [o]

A. Bertolin, R. Brugnera, R. Carlin, F. Dal Corso, S. Dusini, S. Limentani, A. Longhin, M. Posocco, L. Stanco, M. Turcato
Dipartimento di Fisica dell' Università and INFN, Padova, Italy [f]

L. Adamczyk[23], L. Iannotti[23], B.Y. Oh, J.R. Okrasiński, P.R.B. Saull[23], W.S. Toothacker[12]†, J.J. Whitmore
Pennsylvania State University, Dept. of Physics, University Park, PA, USA [q]

Y. Iga
Polytechnic University, Sagamihara, Japan [g]

G. D'Agostini, G. Marini, A. Nigro
Dipartimento di Fisica, Univ. 'La Sapienza' and INFN, Rome, Italy [f]

C. Cormack, J.C. Hart, N.A. McCubbin, T.P. Shah
Rutherford Appleton Laboratory, Chilton, Didcot, Oxon, U.K. [o]

D. Epperson, C. Heusch, H.F.-W. Sadrozinski, A. Seiden, R. Wichmann, D.C. Williams
University of California, Santa Cruz, CA, USA [p]

I.H. Park
Seoul National University, Seoul, Korea

N. Pavel
Fachbereich Physik der Universität-Gesamthochschule Siegen, Germany [c]

H. Abramowicz[24], S. Dagan[25], S. Kananov[25], A. Kreisel, A. Levy[25]
Raymond and Beverly Sackler Faculty of Exact Sciences, School of Physics, Tel-Aviv University, Tel-Aviv, Israel [e]

T. Abe, T. Fusayasu, T. Kohno, K. Umemori, T. Yamashita
Department of Physics, University of Tokyo, Tokyo, Japan [g]

R. Hamatsu, T. Hirose, M. Inuzuka, S. Kitamura[26], K. Matsuzawa, T. Nishimura
Tokyo Metropolitan University, Dept. of Physics, Tokyo, Japan [g]

M. Arneodo[27], N. Cartiglia, R. Cirio, M. Costa, M.I. Ferrero, S. Maselli, V. Monaco, C. Peroni, M. Ruspa, R. Sacchi, A. Solano, A. Staiano
Università di Torino, Dipartimento di Fisica Sperimentale and INFN, Torino, Italy [f]

D.C. Bailey, C.-P. Fagerstroem, R. Galea, T. Koop, G.M. Levman, J.F. Martin, A. Mirea, A. Sabetfakhri
University of Toronto, Dept. of Physics, Toronto, Ont., Canada [a]

J.M. Butterworth, C.D. Catterall, M.E. Hayes, E.A. Heaphy, T.W. Jones, J.B. Lane, B.J. West
University College London, Physics and Astronomy Dept., London, U.K. [o]

J. Ciborowski, R. Ciesielski, G. Grzelak, R.J. Nowak, J.M. Pawlak, R. Pawlak, B. Smalska, T. Tymieniecka, A.K. Wróblewski, J.A. Zakrzewski, A.F. Żarnecki
Warsaw University, Institute of Experimental Physics, Warsaw, Poland [j]

M. Adamus, T. Gadaj
Institute for Nuclear Studies, Warsaw, Poland [j]

O. Deppe, Y. Eisenberg, D. Hochman, U. Karshon[25]
Weizmann Institute, Department of Particle Physics, Rehovot, Israel [d]

W.F. Badgett, D. Chapin, R. Cross, C. Foudas, S. Mattingly, D.D. Reeder, W.H. Smith, A. Vaiciulis[28], T. Wildschek, M. Wodarczyk
University of Wisconsin, Dept. of Physics, Madison, WI, USA [p]

A. Deshpande, S. Dhawan, V.W. Hughes
Yale University, Department of Physics, New Haven, CT, USA [p]

S. Bhadra, C. Catterall, J.E. Cole, W.R. Frisken, R. Hall-Wilton, M. Khakzad, S. Menary
York University, Dept. of Physics, Toronto, Ont., Canada [a]

[1] now visiting scientist at DESY
[2] now at Univ. of Salerno and INFN Napoli, Italy
[3] now at CERN
[4] now at CalTech, USA
[5] now at Sparkasse Bonn, Germany
[6] now at Siemens ICN, Berlin, Germanny
[7] retired
[8] supported by the GIF, contract I-523-13.7/97
[9] PPARC Advanced fellow
[10] supported by the Portuguese Foundation for Science and Technology (FCT)
[11] now at Dongshin University, Naju, Korea
[12] deceased
[13] now at Netlife AG, Hamburg, Germany
[14] now at University of Edinburgh, Edinburgh, U.K.
[15] partly supported by an ICSC-World Laboratory Björn H. Wiik Scholarship
[16] visitor of Univ. of Crete, Greece, partially supported by DAAD, Bonn - Kz. A/98/16764
[17] on leave from MSU, supported by the GIF, contract I-0444-176.07/95
[18] supported by DAAD, Bonn - Kz. A/98/12712
[19] also at University of Tokyo
[20] supported by the Comunidad Autonoma de Madrid
[21] now at Loma Linda University, Loma Linda, CA, USA
[22] supported by the Feodor Lynen Program of the Alexander von Humboldt foundation
[23] partly supported by Tel Aviv University
[24] an Alexander von Humboldt Fellow at University of Hamburg
[25] supported by a MINERVA Fellowship
[26] present address: Tokyo Metropolitan University of Health Sciences, Tokyo 116-8551, Japan
[27] now also at Università del Piemonte Orientale, I-28100 Novara, Italy
[28] now at University of Rochester, Rochester, NY, USA

[a] supported by the Natural Sciences and Engineering Research Council of Canada (NSERC)

[b] supported by the FCAR of Québec, Canada

[c] supported by the German Federal Ministry for Education and Science, Research and Technology (BMBF), under contract numbers 057BN19P, 057FR19P, 057HH19P, 057HH29P, 057SI75I

[d] supported by the MINERVA Gesellschaft für Forschung GmbH, the Israel Science Foundation, the U.S.-Israel Binational Science Foundation, the Israel Ministry of Science and the Benozyio Center for High Energy Physics

[e] supported by the German-Israeli Foundation, the Israel Science Foundation, the U.S.-Israel Binational Science Foundation, and by the Israel Ministry of Science

[f] supported by the Italian National Institute for Nuclear Physics (INFN)

[g] supported by the Japanese Ministry of Education, Science and Culture (the Monbusho) and its grants for Scientific Research

[h] supported by the Korean Ministry of Education and Korea Science and Engineering Foundation

[i] supported by the Netherlands Foundation for Research on Matter (FOM)

[j] supported by the Polish State Committee for Scientific Research, grant No. 112/E-356/SPUB/DESY/P03/DZ 3/99, 620/E-77/SPUB/DESY/P-03/ DZ 1/99, 2P03B03216, 2P03B04616, 2P03B03517, and by the German Federal Ministry of Education and Science, Research and Technology (BMBF)

[k] supported by the Polish State Committee for Scientific Research (grant No. 2P03B08614 and 2P03B06116)

[l] partially supported by the German Federal Ministry for Education and Science, Research and Technology (BMBF)

[m] supported by the Fund for Fundamental Research of Russian Ministry for Science and Education and by the German Federal Ministry for Education and Science, Research and Technology (BMBF)

[n] supported by the Spanish Ministry of Education and Science through funds provided by CICYT

[o] supported by the Particle Physics and Astronomy Research Council

[p] supported by the US Department of Energy

[q] supported by the US National Science Foundation

1 Introduction

A wealth of data [1–10] exists on charge-exchange processes in soft hadronic reactions, where an initial-state proton is transformed into a final-state neutron, $p \to n$. A successful phenomenological description of these results has been obtained with the concept of the exchange of virtual isovector mesons, such as π, ρ, and a_2, using Regge theory [11–17]. Since the pion is by far the lightest hadron, its exchange dominates the $p \to n$ transition, particularly at small values of the squared momentum transfer, t, between the proton and the neutron.

The assumption of factorization, namely that the partonic nature of a hadron is independent of the hard scattering process in which it participates, has been shown to be valid in the case of the nucleon, whose partonic structure has been probed extensively in jet-production processes as well as in deep inelastic scattering. The idea of factorization may be extended to the exchanged objects in charge-exchange reactions. Under this assumption, hard processes occurring in charge-exchange reactions, such as the production of high-E_T jets, provide a means of investigating the partonic nature of the exchanged objects.

Charge-exchange processes have been studied in deep inelastic scattering at HERA [18,19]. This paper reports the first observation of the photoproduction of dijets in association with an energetic forward neutron:

$$e^+ + p \to e^+ + n + \text{jet} + \text{jet} + X_r \tag{1}$$

where X_r denotes the remainder of the final state. The virtuality of the exchanged photon, Q^2, was less than ~ 4 GeV^2, with a median value of about 10^{-3} GeV^2. Neutrons with energy $E_n > 400$ GeV and produced at an angle $\theta_n < 0.8$ mrad with respect to the direction[1] of the HERA proton beam ($E_p = 820$ GeV) were detected in a forward neutron calorimeter. These results extend previous ZEUS photoproduction dijet studies [20–22].

The present data are compared to an inclusive sample of dijet events selected without the requirement of a forward neutron. Cross sections are presented both as a function of the kinematic variables of the jet and of the $p \to n$ transition. The contributions to the cross section of direct processes, where the photon acts as a point particle, and resolved, where the photon acts as a source of partons, are compared in both the neutron-tagged and the inclusive samples. In addition, the fraction of the inclusive dijet sample with a leading neutron is given as a function of the jet transverse energy ($E_{\rm T}^{\rm jet}$) and pseudorapidity ($\eta^{\rm jet}$). These fractions are used to study the factorization properties of the processes. The results are compared to predictions of one-pion exchange.

[1] The ZEUS coordinate system is defined as right-handed with the Z axis pointing in the proton beam direction, hereafter referred to as forward, and the X axis horizontal, pointing towards the center of HERA. Pseudorapidity is defined as $\eta = -\ln(\tan(\theta/2))$, where the polar angle θ is taken with respect to the proton beam direction.

2 Event kinematics

The dijet processes under consideration here are characterized by an initial state consisting of a positron e^+, and a proton p, and a final state consisting of the scattered positron, the scattered neutron n, and a hadronic system H:

$$e^+(k) + p(P) \rightarrow e^+(k') + n(P') + H \tag{2}$$

where k, k', P and P' are the four-momenta of the initial and scattered positron, and the proton and neutron, respectively. The process is described by four Lorentz invariants. Two describe the positron-photon vertex and can be taken to be the virtuality of the exchanged photon (Q^2) and the electron's inelasticity (y), defined by:

$$Q^2 = -q^2 = -(k - k')^2 \tag{3}$$

$$y = \frac{P \cdot q}{P \cdot k} \tag{4}$$

In photoproduction, where Q^2 is small, $y = (E_e - E')/E_e = E_\gamma/E_e$, where $E_e(E')$ is the energy of the initial (scattered) positron, and E_γ is the incident photon energy. The other two variables, which describe the proton-neutron vertex, are the fraction of the energy of the initial-state proton carried by the neutron ($x_{\rm L}$), and the square of the momentum transfer (t) between the initial proton and the produced neutron, defined by:

$$x_{\rm L} = \frac{P' \cdot k}{P \cdot k} \simeq \frac{E_n}{E_p} \tag{5}$$

$$t = (q')^2 = (P - P')^2 \tag{6}$$

where E_p is the energy of the incident proton. The transverse momentum, $p_{\rm T}$, of the neutron is related to t and $x_{\rm L}$ by:

$$t = -\frac{p_{\rm T}^2}{x_{\rm L}} - \frac{(1 - x_{\rm L})(m_n^2 - x_{\rm L} m_p^2)}{x_{\rm L}} \tag{7}$$

where $m_p(m_n)$ is the mass of the proton (neutron).

In the photoproduction of dijets tagged with a leading neutron, the hadronic system H contains at least two jets:

$$e^+(k) + p(P) \;\rightarrow\; e^+(k') + n(P') + H \;\rightarrow\; e^+(k') + n(P') + \text{jet} + \text{jet} + X_r \tag{8}$$

In $2 \rightarrow 2$ scattering of massless partons, the fractions of the four-momenta $q = (k - k')$ and $q' = (P - P')$ carried into the hard scattering by the initial-state partons are given by:

$$x_\gamma = \frac{(p_{J1} + p_{J2}) \cdot q'}{q \cdot q'} \tag{9}$$

$$x_\pi = \frac{(p_{J1} + p_{J2}) \cdot q}{q \cdot q'} \tag{10}$$

respectively, where p_{Ji} is the four-momentum of the ith final-state parton, and the approximation $q^2 \approx (q')^2 \approx 0$ has been used. The energy fraction contributed by the exchanged photon to the production of the dijets is x_γ; in Regge models, where $p \to n$ is the result of the π, ρ or a_2 trajectory coupling to the pn vertex, the corresponding contribution of the exchanged meson is x_π. A further relationship is:

$$x_\pi = x_p/(1 - x_{\rm L}) \tag{11}$$

where x_p is the fraction of the proton energy participating in the production of the dijets.

The observables $x_\gamma^{\rm OBS}$, $x_p^{\rm OBS}$ and $x_\pi^{\rm OBS}$, defined in terms of jets, are introduced [20]:

$$x_\gamma^{\rm OBS} = \frac{\sum_{\rm jets} E_{\rm T}^{\rm jet} e^{-\eta^{\rm jet}}}{2E_\gamma} \tag{12}$$

$$x_p^{\rm OBS} = \frac{\sum_{\rm jets} E_{\rm T}^{\rm jet} e^{\eta^{\rm jet}}}{2E_p} \tag{13}$$

$$x_\pi^{\rm OBS} = \frac{x_p^{\rm OBS}}{(1 - x_{\rm L})} \tag{14}$$

where the sum runs over the two jets of highest $E_{\rm T}^{\rm jet}$ in an event. The variables $x_\gamma^{\rm OBS}$ and $x_\pi^{\rm OBS}$ are estimators of x_γ and x_π, respectively.

In leading-order (LO) QCD, two types of processes contribute to jet photoproduction [23,24]: either the entire photon interacts with a parton in the target (the *direct* process), or the photon acts as a source of partons which scatter off those in the target (the *resolved* process). Figure 1 illustrates these processes for reaction (8) with an assumed meson-exchange contribution. The observable $x_\gamma^{\rm OBS}$ is sensitive to which type of process occurs [25]. Direct processes are concentrated at high values of $x_\gamma^{\rm OBS}$, resolved processes at low values.

3 Experimental conditions

The data sample used in this analysis was collected in 1995 with the ZEUS detector using e^+p interactions. In this period HERA operated with 174 colliding bunches of $E_p = 820$ GeV protons and $E_e = 27.5$ GeV positrons, corresponding to a center-of-momentum-frame energy $\sqrt{s} = 300$ GeV. Additionally, 21 unpaired bunches of protons or positrons allowed the beam–related backgrounds to be determined. The integrated luminosity used in this analysis is 6.4 pb^{-1}.

The ZEUS detector is described in detail elsewhere [26]. The principal components used in the present analysis were the central tracking detector (CTD) [27] positioned in a 1.43 T

solenoidal magnetic field, the uranium-scintillator sampling calorimeter (CAL) [28], and the forward neutron calorimeter (FNC) [29]. The tracking system was used to establish an interaction vertex with a typical resolution along (transverse to) the beam direction of 0.4(0.1) cm. Energy deposits in the CAL were used to find jets and to measure their energies and angles. The CAL is hermetic and consists of 5918 cells, each read out by two photomultiplier tubes. Under test beam conditions, the CAL has energy resolutions of $\sigma(E) = 18\%\sqrt{E}$ for electrons and $35\%\sqrt{E}$ for hadrons (E in GeV) [28]. Jet energies were corrected for the energy lost in inactive material (typically one radiation length) in front of the CAL.

3.1 Forward neutron calorimeter

The forward neutron calorimeter [29] was installed in the HERA tunnel at $\theta = 0$ degrees and at $Z = 106$ m from the interaction point in the proton-beam direction, and used for the 1995 data taking. The layout of the calorimeter is shown in Fig. 2. The FNC is a sampling calorimeter with 134 layers of 1.25 cm thick lead as the absorber and 0.26 cm thick scintillator as the active material. The scintillator is read out on each side with wavelength-shifting light-guides coupled to photomultiplier tubes. It is segmented longitudinally into a front section, seven interaction-lengths deep, and a rear section, three interaction-lengths deep. The front section is divided vertically into 14 towers, allowing the separation of electromagnetic and hadronic showers using the energy-weighted vertical width of the showers. The energy resolution for hadrons, as measured in a beam test, is $65\%\sqrt{E}$ (E in GeV) [29]. Neutrons are easily distinguished from protons, which are deflected upwards by the beam magnets and deposit most of their energy in the top four towers of the FNC.

Three planes of veto counters, each $70 \times 50 \times 2$ cm^3, are located 70, 78, and 199 cm in front of the calorimeter. These counters, which completely cover the bottom front face of the calorimeter, were used offline to identify charged particles and so reject particles which interacted in the inactive material in front of the FNC.

Magnet apertures limit the FNC acceptance to neutrons with production angles less than 0.8 mrad, that is to transverse momenta $p_{\rm T} \leq E_n\theta_{\rm max} = 0.66x_{\rm L}$ GeV. Only about one quarter of the corresponding azimuth is free of obstruction, as can be seen from the outline of the aperture in Fig. 2(a). The Z-axis intersection with the FNC is also indicated. The overall acceptance of the FNC, which includes beam-line geometry, absorbing material, and the angular distribution of the neutrons, is about 30% for neutrons with energy $E_n > 400$ GeV and $\theta_n < 0.8$ mrad. The kinematic region covered by the FNC in longitudinal and transverse variables is shown in Fig. 3. Although the acceptance extends to $p_{\rm T}^2 \simeq 0.4$ GeV^2, the mean value of $p_{\rm T}^2$ for the accepted data is less

than 0.05 GeV^2 [30]. The t acceptance is strongly affected by the minimum value of $|t|$, $t_{\rm min} = (1 - x_{\rm L})(m_n^2 - x_{\rm L} m_p^2)/x_{\rm L}$.

The calibration and monitoring [31] of the FNC follow the methods developed for the FNC test calorimeters [18, 32]. The gain of the photomultiplier tubes is obtained by scanning the FNC with a ^{60}Co radioactive source. Changes in gain during data taking are monitored using energy deposits from interactions of the HERA proton beam with residual gas in the beam pipe. The overall energy scale is set from the kinematic end point of 820 GeV by fitting proton beam-gas interaction data with energy greater than 600 GeV to that expected from one-pion exchange [13, 33].

4 Data selection

The ZEUS detector uses a three-level trigger system. At the first level, events were selected by a coincidence of a regional or transverse energy sum in the calorimeter, and at least one track from the interaction point measured in the CTD. At the second level, at least 8 GeV total transverse energy, excluding the eight calorimeter towers immediately surrounding the forward beam pipe, was required and cuts on calorimeter energies and timing were used to suppress events caused by beam-gas interactions [34]. At the third level, a cone algorithm used the calorimeter cell energies and positions to identify jets. Events were required to have at least two jets, each of which satisfied the requirement $E_{\rm T}^{\rm jet} > 3.5$ GeV and $\eta^{\rm jet} < 2.0$, or $E_{\rm T}^{\rm jet} > 4.0$ GeV and $2.0 < \eta^{\rm jet} < 2.5$. Additional tracking cuts were made to reject proton beam-gas interactions and cosmic-ray events. No requirement on the FNC was made at any trigger level.

Further selection criteria were applied offline. Charged current scattering events were rejected by a cut on the missing transverse momentum measured in the calorimeter. To reject remaining beam-gas and cosmic-ray backgrounds, tighter cuts were applied. These used the final Z-vertex position, other tracking information and timing information. Two additional cuts were also made [35]:

- events with a well-identified positron candidate in the uranium calorimeter were removed.
- a cut was made on the Jacquet-Blondel estimator of y [36], $y_{JB} = \sum_i (E_i - E_{Z,i})/2E_e$, where $E_{Z,i} = E_i \cos\theta_i$, and E_i is the energy deposited in the calorimeter cell i with a polar angle θ_i with respect to the measured Z-vertex of the event. The sum runs over all calorimeter cells. For any event where the scattered positron entered the uranium calorimeter and was not well identified, the value of y_{JB} is close to one. Proton beam-gas events have low values of y_{JB}. To reduce further the contamination from this

source, it was required that $0.15 < y_{JB} < 0.7$. This range corresponds approximately to a true y range of $0.2 < y < 0.8$, and so to a energy range of $134 < W < 269$ GeV in the γp center-of-momentum frame.

These cuts restricted the range of Q^2 to be less than ~ 4 GeV^2, with a median value of about 10^{-3} GeV^2.

Dijet candidates were selected using the KTCLUS [37] jet algorithm (details can be found in a previous ZEUS publication [21]). Cone [38] algorithms were also used as a check: the conclusions did not change. The jet transverse energy measured in the ZEUS detector was corrected as a function of pseudorapidity and transverse energy to account for energy lost in inactive material. This correction was derived from the Monte Carlo (MC) simulation described in the next section. After all cuts, the kinematic region under study is defined by: $E_{\rm T}^{\rm jet} > 6$ GeV, $|\eta^{\rm jet}| < 2$, $Q^2 < 4$ GeV^2 and $0.2 < y < 0.8$.

Events with a leading neutron were selected from the inclusive dijet sample by requiring a large energy deposit (> 400 GeV) in the FNC. The segmentation of the FNC permits the identification of protons, photons, and neutrons. Scattered protons are bent into the top towers (11-14) by the HERA dipole magnets. As seen in Fig. 2, the geometric aperture of the FNC for neutral particles at normal incidence is centered on towers 7 and 8. Scattered protons were eliminated from the sample by requiring that the tower with the maximum energy deposit be either 6,7,8 or 9. Although both photons and neutrons produce large energy deposits in the bottom section (towers 1-10), the vertical spread of electromagnetic showers is much less than that of hadronic showers. Photons were removed by eliminating showers with a small vertical spread (≤ 3 cm). Finally, neutrons that started showering in front of the FNC were removed by requiring that the scintillator veto counter farthest from the FNC had an energy deposit below that of a minimum-ionizing particle. Only the farthest counter was used, to minimize false vetoes due to calorimeter albedo. Showers with spreads greater than 7.5 cm were also removed since they are inconsistent with originating from a single high-energy hadron.

After these cuts, 1921 events with a neutron remained, comprising approximately 1% (before correction for the FNC acceptance) of the inclusive dijet sample of $2 \cdot 10^5$ events.

5 Monte Carlo simulation

Monte Carlo simulations were used to correct the data for acceptance and for smearing of the measured quantities due to the finite resolution of the detector. For all generated events, the ZEUS detector response was simulated in detail using a program based on GEANT3.13 [39], and the Monte Carlo events were subjected to the same analysis chain

as the data. For the inclusive dijet analysis, the data were compared to Monte Carlo simulations based on PYTHIA5.7 [40] and HERWIG5.9 [41], which include leading-order QCD calculations. A minimum cut-off value $\hat{p}_{\mathrm{T}}^{\mathrm{min}}$ of 2.5 GeV was applied at the MC generator level to the transverse momenta of the outgoing partons in the hard scattering process. The HERWIG event generator was used to check the PYTHIA results. In PYTHIA, the photon flux is calculated using the Weizsäcker-Williams approximation. The parton densities used were GRV LO [42] for the photon and CTEQ4 LO [43] for the proton. The hadronization in PYTHIA was performed using the LUND string model as implemented in JETSET [44]. In HERWIG, the hadronization of partons is based on a cluster model. For comparison, the LAC1 [45] parameterization for the photon and MRSA LO [46] for the proton were also used.

Previous studies have shown that including a simulation of multiparton interactions (MI) in the parton shower programs significantly improves the description of jet production in the forward region [21]. This option, which applies only to resolved processes, adds interactions between the partons in the remnants of the proton and photon, calculated as LO QCD processes, to the hardest scattering process of the event. It was implemented in the HERWIG simulation [47].

The energy corrections for jets were determined from the Monte Carlo samples by comparing the true transverse energy of a jet (found by applying the algorithm to the final state particles) to the transverse energy measured in the calorimeter simulation. The correction to the jet energies was on average +17%, varying between +10% and +25% depending upon η^{jet}. The largest corrections occurred at boundaries within the calorimeter. No correction was applied to the jet pseudorapidity, since the average shift in η between the true and detected jets was less than ± 0.05 for all η values in the range used for the cross section measurements. In each event, the two jets with the highest transverse energies were selected.

For the dijet events with a neutron tag ($E_n > 400$ GeV), the data were corrected using Monte Carlo programs based on POMPYT2.5 [48] and RAPGAP2.06 [49]. These simulations include pion-exchange processes where a virtual pion is emitted from the incoming proton (see Appendix). As discussed later, such a model reproduces the characteristics of the data. The POMPYT generator makes use of the program PYTHIA to simulate $e^+\pi^+$ interactions via resolved and direct photon processes. These programs simulate higher order effects through the use of leading-order parton showers. Hadronization processes are implemented by JETSET (the LUND string model). In both programs GRV-LO was used for the parton densities of the photon and SMRS-P3 [50] for the parton densities of the pion.

The conclusions are independent of the Monte Carlo model used for the corrections: the jet energy corrections and acceptance calculations, both inclusive and neutron-tagged,

can be performed with any of the four Monte Carlo programs (POMPYT, RAPGAP, HERWIG, PYTHIA) without significant change in the results.

6 Systematic uncertainties

A detailed study of the sources contributing to the systematic uncertainties of the measurements was carried out [51]. Those associated with the CTD and CAL, which impact on the jet measurement, and those associated with the FNC, which impact on the neutron measurement, are considered separately.

For the jet measurements, the uncertainties are grouped into the following classes:

- absolute energy scale of the CAL: the energy scale uncertainty of the low E_T CAL jets used in this study is 5%, leading to an uncertainty of 15 to 20% on the cross section;
- model dependence: for the inclusive dijet cross section, the jet-acceptance correction was performed using HERWIG instead of PYTHIA. For the neutron-tagged sample, the acceptance correction was changed from POMPYT to RAPGAP. The associated uncertainties were at the 5% level;
- parton parameterization: changing the parton densities of the proton (CTEQ to MRSA) contributed an uncertainty of 0.4%; changing the parton densities of the photon (GRV to LAC1) 2%;
- event selection: variation of each selection cut by one standard deviation of the resolution gave uncertainties of about 5%.

The main systematic uncertainties associated with the FNC were:

- absolute energy scale of the FNC: the uncertainty on the FNC energy scale is $\pm 2\%$ [31]. This introduced a 1.5% normalization uncertainty on the cross section;
- beam-gas background: charge-exchange processes for beam-gas interactions can produce a high-energy nucleon which might overlap with a dijet event. The uncertainty in the correction of 2% is less than 1%;
- event selection: veto-counter noise (from beam halo and calorimeter albedo) and veto-counter inefficiencies resulted in a 2.5% uncertainty;
- angular distribution of neutrons: the acceptance of the FNC was uncertain due to uncertainties in the angular distribution of the neutrons. The uncertainty in the acceptance was estimated by using different parameterizations of the pion flux. To obtain

a model-independent estimate, the angular distribution at fixed $x_{\rm L}$ was assumed to fall exponentially with $p_{\rm T}^2$, $dN/dp_{\rm T}^2 \propto \exp(-bp_{\rm T}^2)$, and the acceptance and its systematic uncertainty were determined by varying the slope parameter b as a function of $x_{\rm L}$ within the limits allowed by the data [30]. The resulting acceptance uncertainty for neutrons with energy $E_n > 400$ GeV was 5.5%;

- sensitivity of the description of the beam-line: the calculated acceptance of the FNC depends on a complete and accurate description of the proton beam-line between the interaction point and the calorimeter. Both the amount of inactive material and the alignment must be known. The model was tested by comparing the fraction of neutrons in the FNC surviving the selection cuts, according to RAPGAP, to that observed. The discrepancy between the expected and observed fraction gave a normalization uncertainty of 6%.

The dominant systematic uncertainty is that associated with the energy scale of the CAL jets. The statistical errors and the systematic uncertainties were added in quadrature and are shown as error bars in the figures. The systematic uncertainty associated with the absolute energy scale is shown as a shaded band. The systematic uncertainties from the FNC give a 9% normalization uncertainty on the neutron-tagged cross section. Since this uncertainty does not affect the shape of any distribution, it is not included in the figures. In addition, a normalization uncertainty of 1.5% from the luminosity determination was not included; this is not relevant in the measurement of the neutron-tagged to inclusive event-rate ratios.

7 Some results and comparisons

The usual simulation models for hard photoproduction processes such as HERWIG or PYTHIA contain a fraction of events with a leading neutron, although it is not, a priori, expected that such simulations will properly describe particle production in the proton fragmentation region. For leading neutrons produced with high longitudinal momentum and low transverse momentum, particle-exchange models may be more appropriate. In this case the LO cross section can be expressed as:

$$\sigma_{res}^{ep} = \left[\int\int dy dQ^2 f_{\gamma/e}(y,Q^2) \int\int dx_L dt f_{\pi/p}(x_L,t) \sum_{i,j} \int dx_\gamma f_{i/\gamma}(x_\gamma,\mu^2) \int dx_\pi f_{j/\pi}(x_\pi,\mu^2) \right.$$
$$\left. \sum_{k,l} \int d\hat{p}_{\rm T}^2 \frac{d\hat{\sigma}_{i+j\to k+l}}{d\hat{p}_{\rm T}^2}(\hat{s},\hat{p}_{\rm T}^2,\mu^2) \right] \qquad (15)$$

where the exchanged meson is denoted by π, and a sum over all exchanged mesons is implied. The dijet cross section in charge-exchange photoproduction contains contributions

from both the direct and resolved processes. In Eq. (15), $f_{\gamma/e}$ is the splitting function of a positron into a photon and positron, $f_{\pi/p}$ is the splitting function of a proton into a meson and neutron (i.e., the flux of mesons in the proton), $f_{i/\gamma}$ is the density of partons of type i in the photon, and $f_{j/\pi}$ is the density of partons of type j in the meson. The sum in i, j runs over all possible types of partons i present in the photon and j in the meson. The sum in k, l runs over all possible types of final state partons. The term $\hat{\sigma}_{i+j\to k+l}$ is the cross section for the two-body collision $i + j \to k + l$ and depends on the square of the center-of-momentum-frame energy, $\hat{s} = y(1 - x_{\rm L})x_\gamma x_\pi s$, the transverse momentum of the two outgoing partons ($\hat{p}_{\rm T}^2$), and the momentum scale (μ) at which the strong-coupling constant ($\alpha_s(\mu^2)$) is evaluated. For the direct process, Eq. (15) also holds except that $f_{i/\gamma}(x_\gamma)$ is replaced by the Dirac delta function, $\delta(1 - x_\gamma)$, and there is no sum over partons i in the photon.

Equation (15) incorporates the assumption of factorization. In particular, the resolved cross section depends on four "parton" densities and a two-body scattering cross section. The kinematic variables y, $x_{\rm L}$, x_γ and x_π are coupled only through the $\hat{s}$ dependence of the hard-scattering cross section, $\hat{\sigma}$. A priori, the shape of the neutron-tagged jet cross sections depends on the kinematic variables of the neutron. In a complete factorization of the baryon and the photon vertices, however, the shape of x_γ and the jet-variable distributions would not depend either on the presence of a neutron or explicitly on its kinematic variables. Similarly, the energy spectrum of the neutrons would be independent of the photon and jet variables.

Meson-exchange models, in the context of Regge theory, are often used to describe nucleon charge-exchange reactions. Since the mass of the pion is small compared to all other mesons, pion exchange (see Appendix) is expected to dominate the amplitude for the $p \to n$ transition, with small contributions from ρ, a_2, etc. In fact, LO one-pion-exchange models account for both the shape and normalization of the distributions for the neutron-tagged data. Figure 4(a) compares the shape of the uncorrected neutron energy spectrum to the prediction of the one-pion-exchange (OPE) model POMPYT for the monopole and light-cone pion form-factors. The POMPYT OPE model with the light-cone form-factor agrees well with the measured energy spectrum. RAPGAP gives essentially the same prediction. The figure also shows that the monopole choice for the form factor is disfavored. It gives a distribution which is both shifted in energy and too narrow. For this comparison, the SMRS-P3 [50] pion parton densities have been used; however, the predicted shape of the neutron spectrum is insensitive to the choice of parton density of the pion [50, 52–54] (not shown). These parton densities are constrained by dimuon and prompt-photon production data from fixed-target experiments that are sensitive mainly to the valence quark distributions, and the parameterizations are similar in the x_π range studied here.

Figure 4(b) shows a comparison of the shape of the neutron energy distribution with the predictions of the Monte Carlo programs PYTHIA and HERWIG. Neither simulation provides a good description of the data. Moreover, PYTHIA (HERWIG) predicts a leading neutron ($E_n > 400$ GeV) in 2% (0.5%) of the dijet events in comparison with the 4.9±0.4% (after correction for the acceptance of the FNC) observed in the data.

The Monte Carlo models considered here do not contain an explicit diffractive component; however, neutrons can also be produced by the diffractive dissociation of the incoming proton through Pomeron exchange. Monte Carlo studies indicate that such neutrons will have an energy spectrum which agrees qualitatively with that observed in the data. Diffractive processes give rise to a large rapidity gap between the hadronic system and the remnant of the proton, which is either a single proton or a low-mass system with the quantum numbers of the proton. The pseudorapidity of the most-forward hadron ($\eta_{\max}$) in the central detector was used to select diffractive events. Meson exchange can also give rise to events with a large rapidity gap via the Deck mechanism [55] in which the exchanged meson itself scatters diffractively off the incoming photon and escapes undetected down the beam pipe.

Diffractively dissociating protons are expected to account for only a small fraction of the dijet events, both inclusive and neutron-tagged, because the E_T of diffractive events is severely limited by the small fraction of the proton energy carried by the Pomeron ($< 5\%$). In contrast, in neutron production there is on average a much larger fraction of the initial proton energy ($\approx 25\%$) available for jet production. Figure 5(a) shows the $\eta_{\max}$ distribution for both inclusive and neutron-tagged dijet photoproduction, normalized to equal area. The shapes of the two distributions are similar. Although there are differences between the two distributions at large $\eta_{\max}$, this region is insensitive to diffractive processes. Less than 1% of each sample has a large rapidity gap ($\eta_{\max} < 2$). In addition, the distributions of the jet variables, $E_{\rm T}^{\rm jet}$, $\eta^{\rm jet}$, and $x_\gamma^{\rm OBS}$ for events with a large rapidity gap [22] are different from those of the neutron-tagged sample, which strongly resemble the inclusive sample (see Section 8). POMPYT and RAPGAP also reproduce the $\eta_{\max}$ distribution of neutron-tagged events, as seen in Fig. 5(b), although neither Monte Carlo contains an explicit diffractive component.

Neutrons can also be produced indirectly through the production and decay of baryonic resonances. Most prominent of these is the Δ, which is itself produced directly through π, ρ or a_2 exchange, and which can decay via $\Delta^0 \to n\pi^0$ or $\Delta^+ \to n\pi^+$. Monte Carlo studies indicate that such decay neutrons will also have an energy spectrum which agrees qualitatively with the data; however, the study of hadronic interactions [56–59] shows that the $\Delta\pi$ contribution to the Fock state of the proton is approximately half that of $n\pi$ [33,60]. When account is taken of the branching ratio for $\Delta \to n$, such indirect neutron production is small compared to the direct $p \to n$ transition.

It can therefore be concluded that standard fragmentation processes, diffractively dissociating protons, and the decay of the Δ resonance are ruled out as the dominant source of dijet events tagged with a leading neutron. The data will be further compared with the one-pion-exchange model in Section 9.

8 Factorization tests

The differential dijet cross sections as a function of $E_{\rm T}^{\rm jet}$ and $\eta^{\rm jet}$ are shown in Fig. 6(a,b) for the inclusive sample, and in Fig. 6(c,d) for the neutron-tagged sample. The predictions of PYTHIA and HERWIG describe the shape of the $E_{\rm T}^{\rm jet}$ distribution reasonably well. The predictions have been normalized to the measured cross section at high $E_{\rm T}^{\rm jet}$ (>16 GeV) in order to facilitate the shape comparison. For the $\eta^{\rm jet}$ distribution, the Monte Carlo is normalized at small $\eta^{\rm jet}$, $-1.5 < \eta^{\rm jet} < 0$. HERWIG with multiparton interactions is in better agreement with the data than PYTHIA without such interactions.

The study of ratios of neutron-tagged to inclusive cross sections is advantageous since many systematic uncertainties, especially those related to the jet measurements, are greatly reduced. In addition, the ratio provides a quantitative comparison of the shapes of the cross sections, and so tests factorization. That the neutron-tagged and inclusive differential cross sections have similar shapes as a function of $E_{\rm T}^{\rm jet}$ is evident in Fig. 6(e). The cross sections fall by over two orders of magnitude in the range $6 < E_{\rm T}^{\rm jet} < 25$ GeV, but the ratio is approximately constant as a function of $E_{\rm T}^{\rm jet}$. Figure 6(f) shows that the ratio as a function of $\eta^{\rm jet}$ falls slightly with increasing $\eta^{\rm jet}$. The ratios of RAPGAP to PYTHIA and RAPGAP to HERWIG with multiparton interactions are also shown in Figs. 6(e,f). The ratio of RAPGAP to HERWIG is in better agreement with the data, as expected from the cross section comparisons. The agreement of RAPGAP and POMPYT with the tagged data supports factorization, which is built into these MC models.

To test further the factorization properties of the dijet cross section, the neutron-tagged and inclusive samples were divided into bins of $x_\gamma^{\rm OBS}$ and $E_{\rm T}^{\rm jet}$. The shape of the observed energy spectrum of the neutron is approximately independent of $x_\gamma^{\rm OBS}$ and $E_{\rm T}^{\rm jet}$, as seen in Fig. 7(a) and (b). Moreover, in a given bin of $x_\gamma^{\rm OBS}$, the fraction of events with a leading neutron is approximately independent on $E_{\rm T}^{\rm jet}$, as seen in Fig. 7(c).

The $x_\gamma^{\rm OBS}$ distribution is determined by the parton densities in the colliding particles, kinematic factors, and a possible presence of interactions between the hadron remnants. Figures 8(a,b) show the uncorrected $x_\gamma^{\rm OBS}$ distribution for inclusive and neutron-tagged events, respectively. The corresponding ratio of neutron-tagged to inclusive production is shown in Fig. 8(c), corrected only for the acceptance of the FNC. In sharp contrast to the results shown in Fig. 6, the ratio rises with increasing $x_\gamma^{\rm OBS}$. The rise is only partially

explained by the Monte Carlo models. The Monte Carlo predictions are shown area normalized to the data in Figs. 8(a,b); the ratio of RAPGAP to HERWIG normalized at $x_\gamma^{\rm OBS} = 0.5$ is shown in Fig. 8(c).

Figure 8(d) shows the ratio of the resolved ($x_\gamma^{\rm OBS} < 0.75$) and direct ($x_\gamma^{\rm OBS} > 0.75$) photoproduction cross sections as a function of $E_{\rm T}^{\rm jet}$ for inclusive events while Fig. 8(e) show the same quantity for neutron-tagged events. The size of the direct component increases with $E^{\rm jet}$ for both the neutron-tagged and the inclusive samples. Overall the direct component is approximately twice as large in the neutron-tagged sample. Figure 8(f) shows that the ratio of the two ratios is constant within errors as a function of $E_{\rm T}^{\rm jet}$ indicating that, although the proportion changes, the shape in $E_{\rm T}^{\rm jet}$ is the same for both samples.

In summary, the shape of the neutron energy spectrum is approximately independent of the the jet variables $E_{\rm T}^{\rm jet}$, $\eta^{\rm jet}$ and $x_\gamma^{\rm OBS}$; the jet variables $E_{\rm T}^{\rm jet}$ and $\eta^{\rm jet}$ are relatively insensitive to the presence of a neutron; however, the ratio of neutron-tagged to inclusive dijet events rates rises with increasing $x_\gamma^{\rm OBS}$.

9 Comparison to a one-pion-exchange model

In the previous two sections, it was shown that standard fragmentation processes, diffractively dissociating protons, and the decay of the Δ resonance are not the dominant source of dijet events tagged with a leading neutron, but that the data are consistent with one-pion exchange and approximately satisfy factorization. It is therefore appropriate in this section to make further comparisons to OPE under the assumption that it is the dominant mechanism for the production of the neutron-tagged events.

The predictions of RAPGAP simulations using the SMRS-P3 parton densities for the pion and the light-cone pion form-factor are in good agreement with the $E_{\rm T}^{\rm jet}$ spectrum for the neutron-tagged events of Fig. 6(c). POMPYT, which is not shown, gives a similar result. Both OPE Monte Carlo models also adequately describe the shape of the $\eta^{\rm jet}$ distribution of Fig. 6(d), where only RAPGAP is shown. The leading-order OPE model is also able to account for the normalization of the data, as shown by the RAPGAP prediction. In contrast to the inclusive case (Fig. 6(b)), the Monte Carlo simulations reproduce the forward $\eta^{\rm jet}$ region without a simulation of multiparton interactions. This comparison suggests that hadron remnant interactions are less important for the neutron-tagged sample, in agreement with naive expectations based on their lower effective center-of-momentum-frame energy compared to the inclusive sample. The RAPGAP and POMPYT simulations are also in fair agreement with the $x_\gamma^{\rm OBS}$ distribution for the neutron-tagged events (Fig. 8(b)). As in the case of the $\eta^{\rm jet}$ distribution, the OPE Monte Carlo models describe the data without simulation of MI, which is needed in the case of the inclusive sample

(Fig. 8(a)). According to the Monte Carlo models, the MI contribution in the inclusive sample strongly increases at low values of $x_\gamma^{\rm OBS}$ [21]. Therefore the ratio of neutron-tagged to inclusive events, which increases with $x_\gamma^{\rm OBS}$ (Fig. 8(c)), can be interpreted to be at least partially caused by the difference in remnant-remnant interactions of the two samples.

The differential cross section for neutron-tagged events as a function of $x_\pi^{\rm OBS}$ (see Eq. 14) is shown in Fig. 9. The measured cross section is compared in Fig. 9 to the predictions of the RAPGAP Monte Carlo model using the light-cone pion form-factor and the SMRS-P3 pion parton densities. The shape of the $x_\pi^{\rm OBS}$ distribution disfavors the monopole form-factor (not shown), but both the shape and normalization are reproduced by both RAPGAP and POMPYT (not shown). The results for other parameterizations of the pion parton densities, which are determined from hadron-hadron interactions, are indistinguishable. The bands show the systematic uncertainty due to the calorimeter energy scale. There is an additional normalization error of 9% which is not shown.

10 Conclusions

Differential cross sections for the inclusive reaction $e^+p \to e^+ + \text{jet} + \text{jet} + X_r$ and the neutron-tagged reaction $e^+p \to e^+ + n + \text{jet} + \text{jet} + X_r$ have been measured in photoproduction for $Q^2 < 4$ GeV^2 and $0.2 < y < 0.8$, with jet transverse energy $E_{\rm T}^{\rm jet} > 6$ GeV, neutron energy $E_n > 400$ GeV and neutron production angle $\theta_n < 0.8$ mrad. Such neutrons are observed in $4.9 \pm 0.4\%$ of the events.

The shape of the neutron energy spectrum is observed to be independent of both $E_{\rm T}^{\rm jet}$ and $x_\gamma^{\rm OBS}$. In addition, the ratio of neutron-tagged to inclusive dijet production rates is approximately independent of the jet transverse energy and pseudorapidity. These observations support the idea of factorization of the positron and proton vertices.

The above ratio does depend on $x_\gamma^{\rm OBS}$, the fraction of the initial photon momentum participating in the hard interaction; the direct to resolved fraction is approximately twice as large in the neutron-tagged sample as in the inclusive sample.

The $x_\gamma^{\rm OBS}$ distribution for the inclusive dijet process can be reproduced in a simulation which includes multiparton interactions. In contrast the neutron-tagged data are well simulated by LO Monte Carlo models including one-pion exchange but without multiparton interactions. These comparisons suggest that the rising ratio of neutron-tagged to inclusive dijet rates as a function of $x_\gamma^{\rm OBS}$ is at least partially due to the difference in remnant-remnant interactions in the two samples.

The standard photoproduction Monte Carlo models, PYTHIA and HERWIG, fail to reproduce either the neutron production rate or the neutron energy spectrum. In contrast,

LO Monte Carlo models such as POMPYT and RAPGAP, which include one-pion exchange and which assume factorization of the pion flux and pion structure, reproduce all aspects of the neutron-tagged data for both the neutron and jet kinematic variables.

Acknowledgments

We are especially grateful to the DESY Directorate whose encouragement and financial support made possible the construction and installation of the FNC. We are also happy to acknowledge the efforts of the DESY accelerator group and the support of the DESY computing group. We thank H. Jung and G. Ingelman for their help with the Monte Carlo programs RAPGAP and POMPYT.

Appendix: pion exchange

Although there are many choices found in the literature for the splitting function of a proton into a pion and neutron, they all can be summarized conveniently in the form [13, 14]:

$$f_{\pi/p}(x_{\rm L}, t) = \frac{1}{4\pi}\frac{g^2_{n\pi p}}{4\pi}\frac{-t}{(m_\pi^2 - t)^2}(1 - x_{\rm L})^{1-2\alpha_\pi(t)}\left(F(x_{\rm L}, t)\right)^2 \tag{16}$$

where $g_{n\pi p}$ is the coupling at the $n\pi p$ vertex, m_π is the mass of the pion, and $\alpha_\pi(t) = \alpha'(t - m_\pi^2)$ is the Regge trajectory of the pion. The trajectory is often omitted by setting the slope constant $\alpha' = 0$, instead of to the measured value, $\alpha' \simeq 1$ GeV^{-2}. $F(x_{\rm L}, t)$ is a form-factor which accounts for final state rescattering of the neutron. Possible choices for the form-factor $F(x_{\rm L}, t)$ are:

$$F(x_{\rm L}, t) = \begin{cases} \exp\left(b(t - m_\pi^2)\right) & \text{Exponential} \\ \exp\left(R^2(t - m_\pi^2)/(1 - x_{\rm L})\right) & \text{Light cone} \\ \left(1 - m_\pi^2/\Lambda^2\right)/\left(1 - t/\Lambda^2\right) & \text{Monopole} \end{cases} \tag{17}$$

where b, R and Λ are constants [33,61,62]. The choice of form-factor depends on whether the pion's Regge trajectory is included or excluded. For the flux with the Regge trajectory the form factor is usually chosen to be an exponential [13]. The light-cone form-factor is usually associated with the flux without the Regge trajectory [17, 63]. These choices are associated with the experimental observation that in hadronic interactions the shape of the $x_{\rm L}$ distribution depends on t [3, 4, 7].

The experimental data are consistent with the flux with the trajectory term included and a constant form factor (that is, $b \approx 0$) [1–10, 13, 14]. Beam-gas data at HERA are also

consistent with a small value for b [31]; Kopeliovich et al [61] use $b = 0.3$ GeV^{-2}. For the light-cone form-factor and the flux without the pion's Regge trajectory, Holtmann et al. [33] take $R = 0.6$ GeV^{-1}. A calculation [64] of the pion form-factor for the one-boson-exchange potential (OBEP) suggests that the monopole with $\Lambda = 0.8$ GeV is a good approximation; however, RAPGAP (see Section 5) takes $\Lambda = 0.5$ GeV [62] and the flux without the Regge trajectory. In the region of the peak of the energy spectrum, $x_{\rm L} \approx 0.7$, the Regge and light-cone splitting functions differ by $\lesssim 10\%$. It should be noted that choices other than those given in Eq. (17) are possible. In particular, recent studies [65, 66] suggest that the the experimental data is best described by a form factor that is hard for small momentum transfers and soft for large momentum transfers.

Other isovector meson exchanges, such as the ρ or a_2, can also contribute to direct neutron production. Recent theoretical studies of neutron production in ep collisions show that processes other than direct pion exchange are expected to contribute $\lesssim 25\%$ of neutron production [33,60,61,67]. These backgrounds to OPE, which increase the rate of neutron production in the FNC phase space, are offset by absorptive rescattering of the neutron, which decreases the rate by approximately the amount of the increase [68, 69]. Also absorptive rescattering preferentially removes neutrons with larger $p_{\rm T}$, increasing the pion contribution relative to the ρ and a_2. Therefore these effects are also neglected in the present analysis.

References

[1] A. R. Erwin et al., Phys. Rev. Lett. 6 (1961) 628.

[2] E. Pickup, D. K. Robinson and E. O. Salant, Phys. Rev. Lett. 7 (1961) 635.

[3] J. Engler et al., Nucl. Phys. B 84 (1975) 70.

[4] B. Robinson et al., Phys. Rev. Lett. 34 (1975) 1475.

[5] W. Flauger and F. Mönnig, Nucl. Phys. B 109 (1976) 347.

[6] J. Hanlon et al., Phys. Rev. Lett. 37 (1976) 967; Phys. Rev. D 20 (1979) 2135.

[7] G. Hartner, Ph. D. Thesis, McGill University, 1977 (unpublished).

[8] Y. Eisenberg et al., Nucl. Phys. B 135 (1978) 189.

[9] V. Blobel et al., Nucl. Phys. B 135 (1978) 379.

[10] H. Abramowicz et al., Nucl. Phys. B 166 (1980) 62.

[11] H. Yukawa, Proc. Phys. Math. Soc. Japan 17 (1935) 48.

[12] J. D. Sullivan, Phys. Rev. D 5 (1972) 1732.

[13] M. Bishari, Phys. Lett. B 38 (1972) 510.

[14] R. D. Field and G. C. Fox, Nucl. Phys. B 80 (1974) 367.

[15] S. N. Ganguli and D. P. Roy, Phys. Rep. 67 (1980) 201.

[16] B. G. Zakharov and V. N. Sergeev, Sov. J. Nucl. Phys. 38 (1983) 947; Sov. J. Nucl. Phys. 39 (1984) 448.

[17] V. R. Zoller, Z. Phys. C 53 (1992) 443.

[18] ZEUS Collaboration, M. Derrick et al., Phys. Lett. B 384 (1996) 388.

[19] H1 Collaboration, C. Adloff et al., Eur. Phys. J. C 6 (1999) 587.

[20] ZEUS Collaboration, M. Derrick et al., Phys. Lett. B 348 (1995) 665.

[21] ZEUS Collaboration, J. Breitweg et al., Eur. Phys. J. C 1 (1998) 109.

[22] ZEUS Collaboration, J. Breitweg et al., Eur. Phys. J. C 5 (1998) 41.

[23] J. F. Owens, Phys. Rev. D 21 (1980) 54.

[24] M. Drees and F. Halzen, Phys. Rev. Lett. 61 (1988) 275;
M. Drees and R. M. Godbole, Phys. Rev. D 39 (1989) 169.

[25] ZEUS Collaboration, M. Derrick et al., Phys. Lett. B 322 (1994) 287.

[26] ZEUS Collaboration, M. Derrick et al., Phys. Lett. B 293 (1992) 465;
ZEUS Collaboration, 'The ZEUS Detector', Status Report 1993, ed. U. Holm, DESY(1993) (unpublished).

[27] N. Harnew et al., Nucl. Instr. and Meth. A 279 (1989) 290;
B. Foster et al., Nucl. Phys. Proc. Suppl. 32 (1993) 181; Nucl. Instr. and Meth. A 338 (1994) 254.

[28] M. Derrick et al., Nucl. Instr. and Meth. A 309 (1991) 77;
A. Andresen et al., Nucl. Instr. and Meth. A 309 (1991) 101;
A. Bernstein et al., Nucl. Instr. and Meth. A 336 (1993) 23.

[29] S. Bhadra et al., Nucl. Instr. and Meth. A 394 (1997) 121.

[30] ZEUS Collaboration, Paper 440 submitted to XXXth International Conference on High Energy Physics, Osaka, Japan, 2000.

[31] ZEUS FNC Group, S. Bhadra et al., in *Proceedings of the Seventh International Conference on calorimetry in High Energy Physics*, Tucson, Arizona, USA, November 9-14, 1997, eds. E. Cheu et al, (World Scientific, Singapore, 1998).

[32] S. Bhadra et al., Nucl. Instr. and Meth. A 355 (1995) 470.

[33] H. Holtmann et al., Phys. Lett. B 338 (1994) 363.

[34] ZEUS Collaboration, M. Derrick et al., Phys. Lett. B 316 (1993) 412.

[35] ZEUS Collaboration, M. Derrick et al., Phys. Lett. B 322 (1994) 287.

[36] F. Jacquet and A. Blondel, in *Proceedings of the study of an ep facility for Europe*, ed. U. Amaldi, (DESY 79/48, Hamburg, 1979) p. 391.

[37] S. Catani et al., Nucl. Phys. B 406 (1993) 187.

[38] J. Huth et al., in *Proceedings of the 1990 DPF Study on High Energy Physics*, Snowmass, Colorado, ed. E. L. Berger (World Scientific, Singapore, 1992) p. 134;
UA1 Collaboration, G. Arnison et al., Phys. Lett. B 123 (1983) 115.

[39] GEANT 3.13, R. Brun et al., CERN DD/EE/84-1 (1987).

[40] H.-U. Bengtsson and T. Sjöstrand, Comp. Phys. Comm. 46 (1987) 43.

[41] G. Marchesini et al., Comp. Phys. Comm. 67 (1992) 465.

[42] M. Glück, E. Reya and A. Vogt, Phys. Rev. D 46 (1992) 1973.

[43] CTEQ Collaboration, J. Botts et al., Phys. Lett. B 304 (1993) 159;
CTEQ Collaboration, H. L. Lai et al., Phys. Rev. D 51 (1995) 4763.

[44] T. Sjöstrand, Comp. Phys. Comm. 82 (1994) 74.

[45] H. Abramowicz, K. Charchula and A. Levy, Phys. Lett. B 269 (1991) 458.

[46] A. D. Martin, W. J. Stirling and R. G. Roberts, Phys. Rev. D 50 (1994) 6734.

[47] J. M. Butterworth, J. R. Forshaw and M. H. Seymour, Z. Phys. C 72 (1996) 637.

[48] P. Bruni and G. Ingelman, Phys. Lett. B 311 (1993) 317;
P. Bruni, A. Edin and G. Ingelman, DESY 93-137 (1993), http://www3.tsl.uu.se/thep/pompyt/.

[49] H. Jung, Comp. Phys. Comm. 86 (1995) 147.

[50] P. J. Sutton et al., Phys. Rev. D 45 (1992) 2349.

[51] M. Khakzad, Ph. D. Thesis, York University, 2000 (DESY-THESIS-2000-008).

[52] J. F. Owens, Phys. Rev. D 30 (1984) 943.

[53] P. Aurenche et al., Phys. Lett. B 233 (1989) 517.

[54] M. Glück, E. Reya and A. Vogt, Z. Phys. C 53 (1992) 651.

[55] S. D. Drell and K. Hiida, Phys. Rev. Lett. 7 (1961) 199;
R. T. Deck, Phys. Rev. Lett. 13 (1964) 169.

[56] J. Erwin et al., Phys. Rev. Lett. 35 (1975) 980.

[57] P. D. Higgins et al., Phys. Rev. D 19 (1979) 731.

[58] S. J. Barish et al., Phys. Rev. D 12 (1975) 1260.

[59] F. T. Dao et al., Phys. Rev. Lett. 30 (1973) 34.

[60] A. W. Thomas and C. Boros, Eur. Phys. J. C 9 (1999) 267.

[61] B. Kopeliovich, B. Povh and I. Potashnikova, Z. Phys. C 73 (1996) 125.

[62] L. L. Frankfurt, L. Mankiewicz and M. I. Strikman, Z. Phys. A 334 (1989) 343.

[63] J. Pumplin, Phys. Rev. D 7 (1973) 795; Phys. Rev. D 8 (1973) 2249.

[64] T. Meissner, Phys. Rev. C 52 (1995) 3386.

[65] G. Holzwarth and R. Machleidt, Phys. Rev. C 55 (1997) 1088.

[66] R. J. Fries and A. Schäfer, Phys. Rev. C 57 (1998) 3470.

[67] N. N. Nikolaev et al., Phys. Rev. D 60 (1999) 014004.

[68] U. D'Alesio and H. J. Pirner, Eur. Phys. J. A 7 (2000) 109.

[69] N. N. Nikolaev, J. Speth and B. G. Zakharov, hep-ph/9708290 (1997).

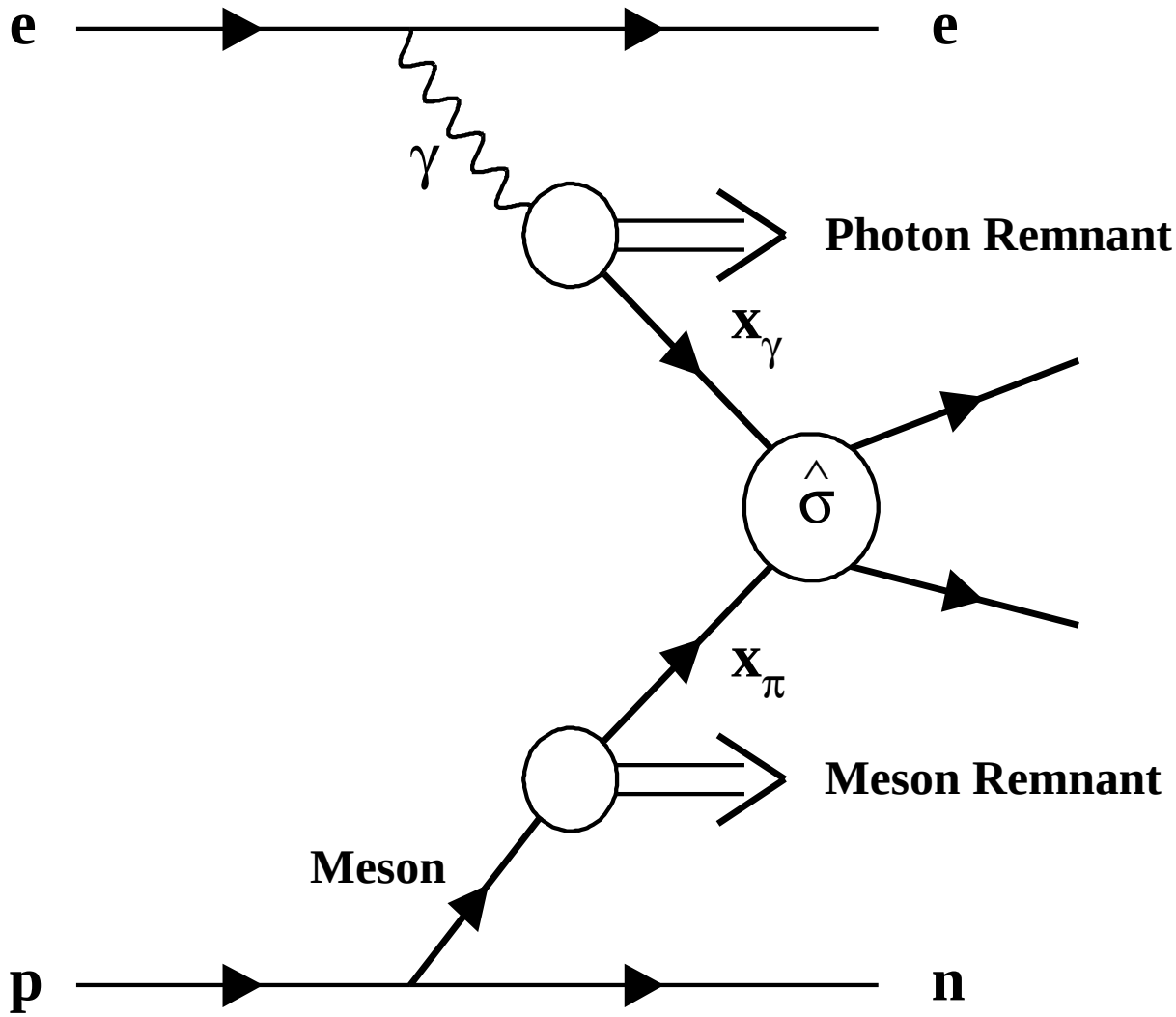

Figure 1: *Resolved photoproduction of dijet events with a leading neutron through meson exchange. The fraction of the energy of the exchanged meson (photon) participating in the partonic hard scattering that produces the dijet system is denoted by x_π (x_γ); the corresponding hard cross section is $\hat{\sigma}$. In direct photoproduction, the entire exchanged photon participates in the hard scattering, there is no photon remnant, and $x_\gamma = 1$.*

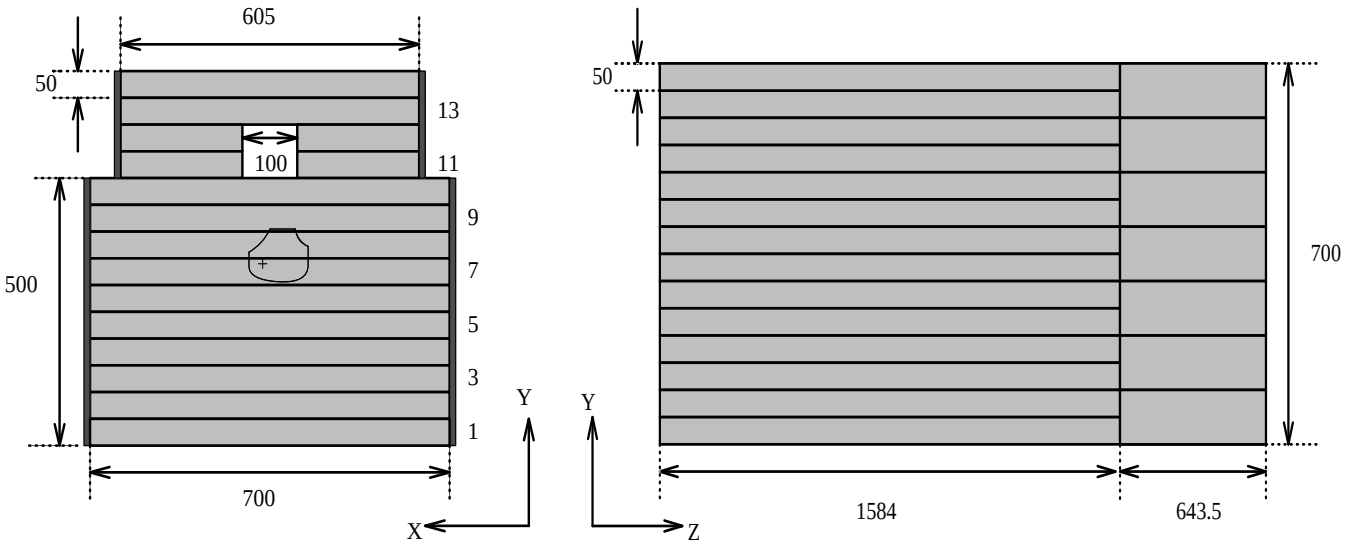

Figure 2: *(a) Front view of the FNC showing the top and bottom sections. The outline in towers 7 and 8 shows the open geometric aperture for the incident neutrons. The point (+) marks zero degrees. The hole in towers 11 and 12 accommodates the proton beam pipe of HERA. The darker shading indicates the location of the wavelength-shifting light-guides. (b) A side view showing the front and rear sections. The vertical segmentation in the front is 50 mm; the segmentation in the rear is 100 mm. All dimensions are in mm.*

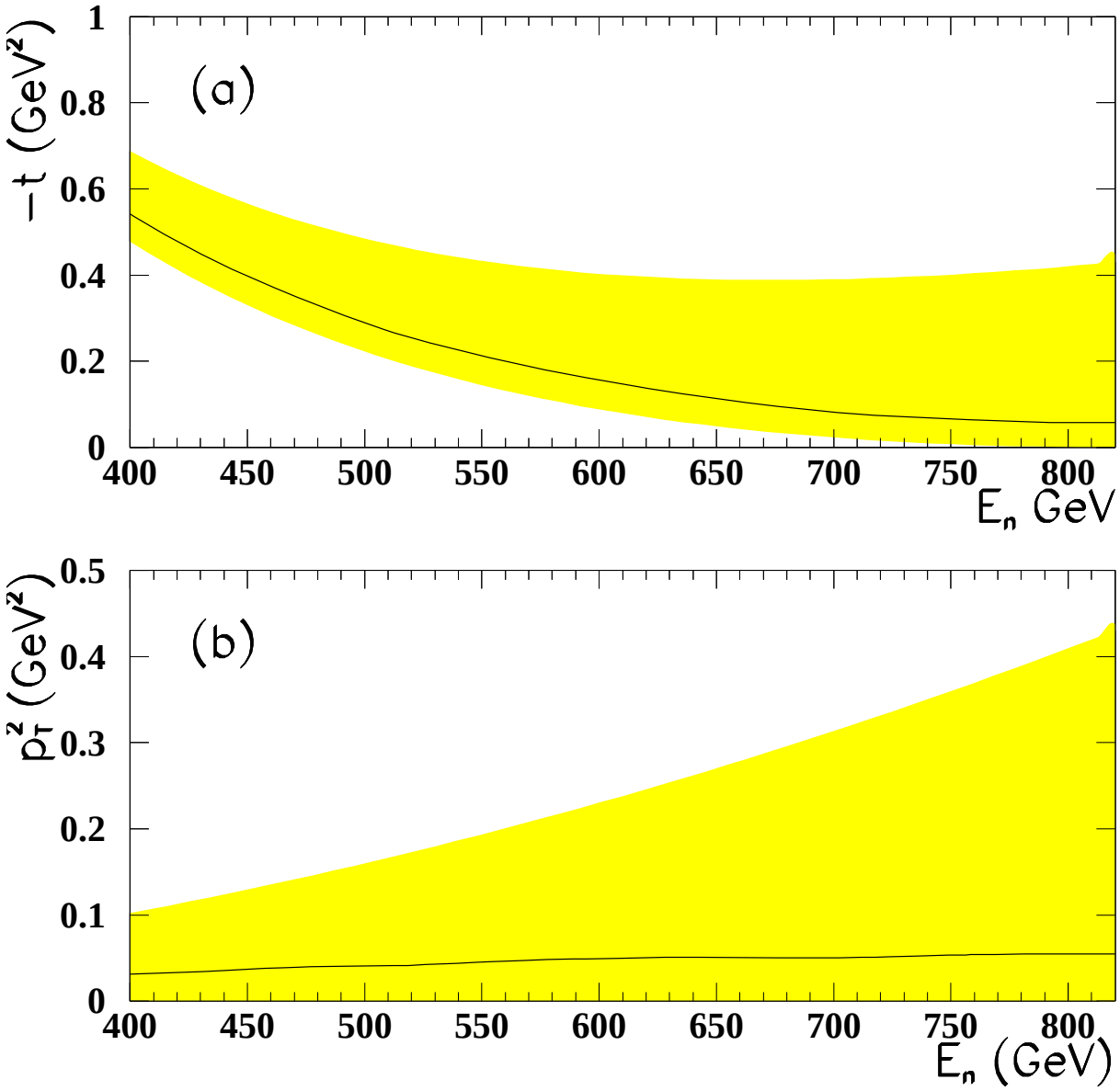

Figure 3: *The kinematic regions in (a) t, and (b) $p_{\rm T}^2$ covered by the angular acceptance of the FNC ($\theta < 0.8$ mrad) are shown as shaded bands. The solid lines show the average t and $p_{\rm T}^2$, respectively, as function of the neutron energy E_n.*

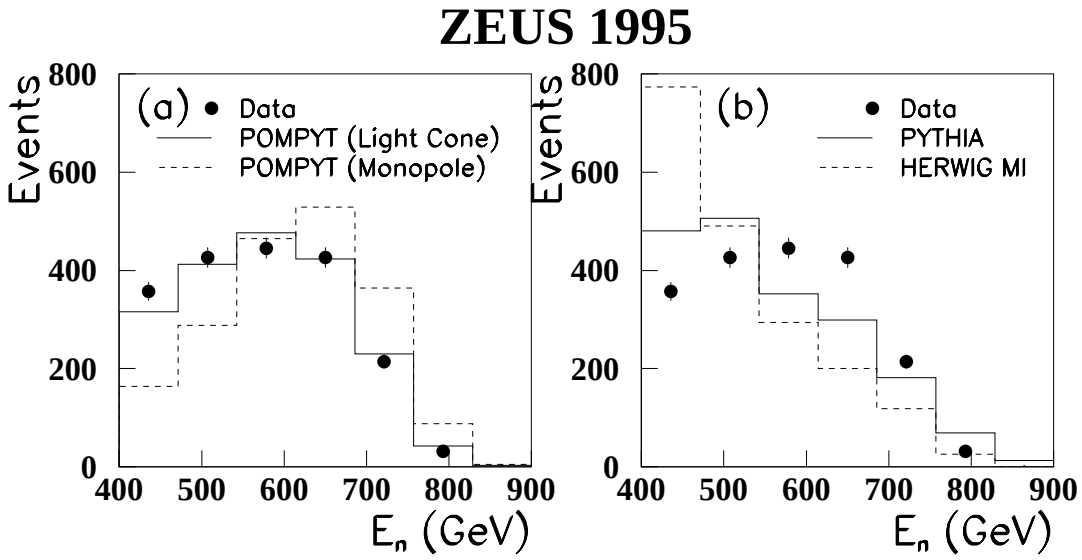

Figure 4: *Comparison of the neutron energy spectrum in dijet events with (a) the predictions of POMPYT for (i) the light-cone and (ii) the monopole pion form-factors and flux without the pion's Regge trajectory, and (b) the predictions of PYTHIA and HERWIG with multiparton interactions. The results for RAPGAP are indistinguishable from those of POMPYT. The energy spectrum is uncorrected for acceptance. The Monte Carlo results, which take into account the acceptance and resolution of the FNC, are area-normalized to the data. Only statistical errors are shown.*

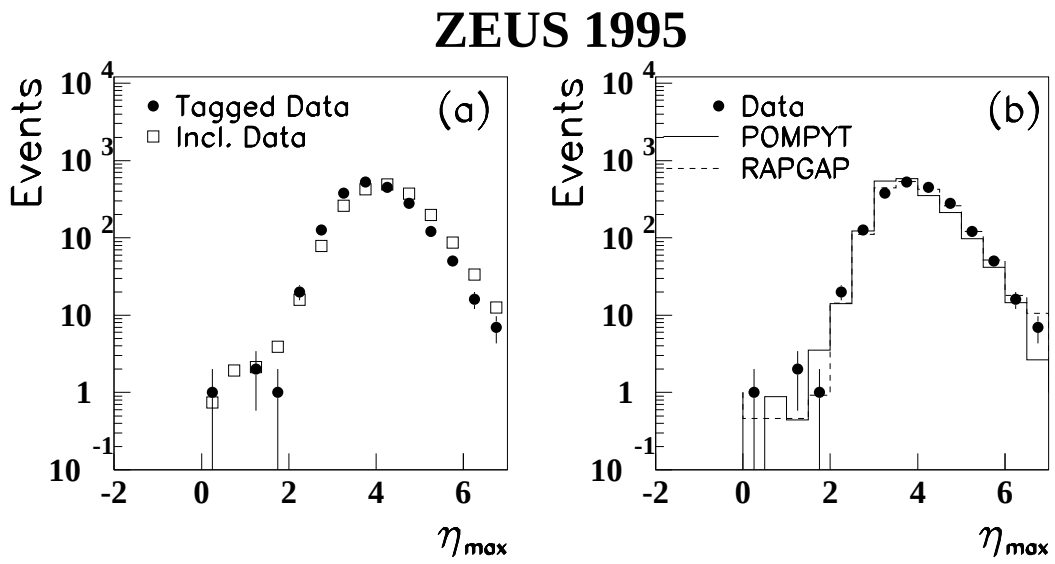

Figure 5: *(a) The $\eta_{\max}$ distribution for neutron-tagged and inclusive dijet photoproduction data. (b) The $\eta_{\max}$ distribution for neutron-tagged dijet photoproduction compared to the predictions of POMPYT and RAPGAP. The inclusive distribution is area normalized to the tagged distribution. Only statistical errors are shown.*

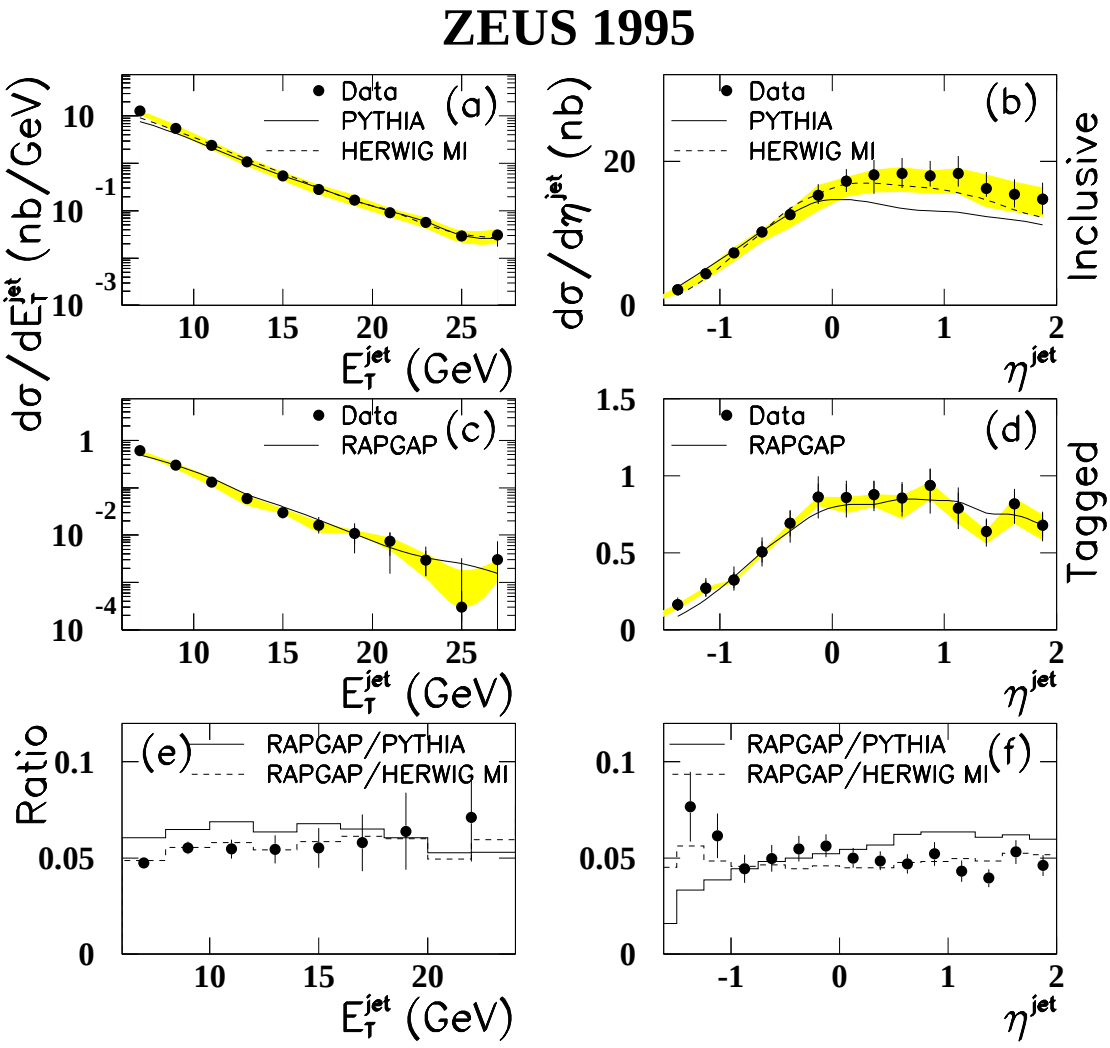

Figure 6: *The differential dijet cross sections as a function of* $E_{\rm T}^{\rm jet}$ *and* $\eta^{\rm jet}$ *for both inclusive (a,b) and neutron-tagged (c,d) photoproduction. The kinematic region studied is* $E_{\rm T}^{\rm jet} > 6$ *GeV,* $|\eta^{\rm jet}| < 2$, $Q^2 < 4$ *GeV*^{2}, $0.2 < y < 0.8$, $E_n > 400$ *GeV, and* $\theta_n < 0.8$ *mrad. For the inclusive cross sections the Monte Carlo predictions have been normalized to the measured cross sections at high* $E_{\rm T}^{\rm jet}$ *and negative* $\eta^{\rm jet}$*, respectively, in order to facilitate the comparison of the shapes. The tagged data are compared with the predictions of the one-pion-exchange model RAPGAP using the SMRS-P3 pion parton densities and the light-cone pion form-factor. The bands show the systematic uncertainty due to the calorimeter energy scale. The error bars show the statistical error added in quadrature with the remaining systematic error. The tagged cross sections have an additional normalization uncertainty of 9% which is not shown. Also shown are the ratio of the cross sections of neutron-tagged to inclusive dijet photoproduction as a function of (e)* $E_{\rm T}^{\rm jet}$*, i.e.* [(c)/(a)]*, and (f)* $\eta^{\rm jet}$*, i.e.* [(d)/(b)]*; and Monte Carlo predictions for the ratio using RAPGAP to PYTHIA and RAPGAP to HERWIG.*

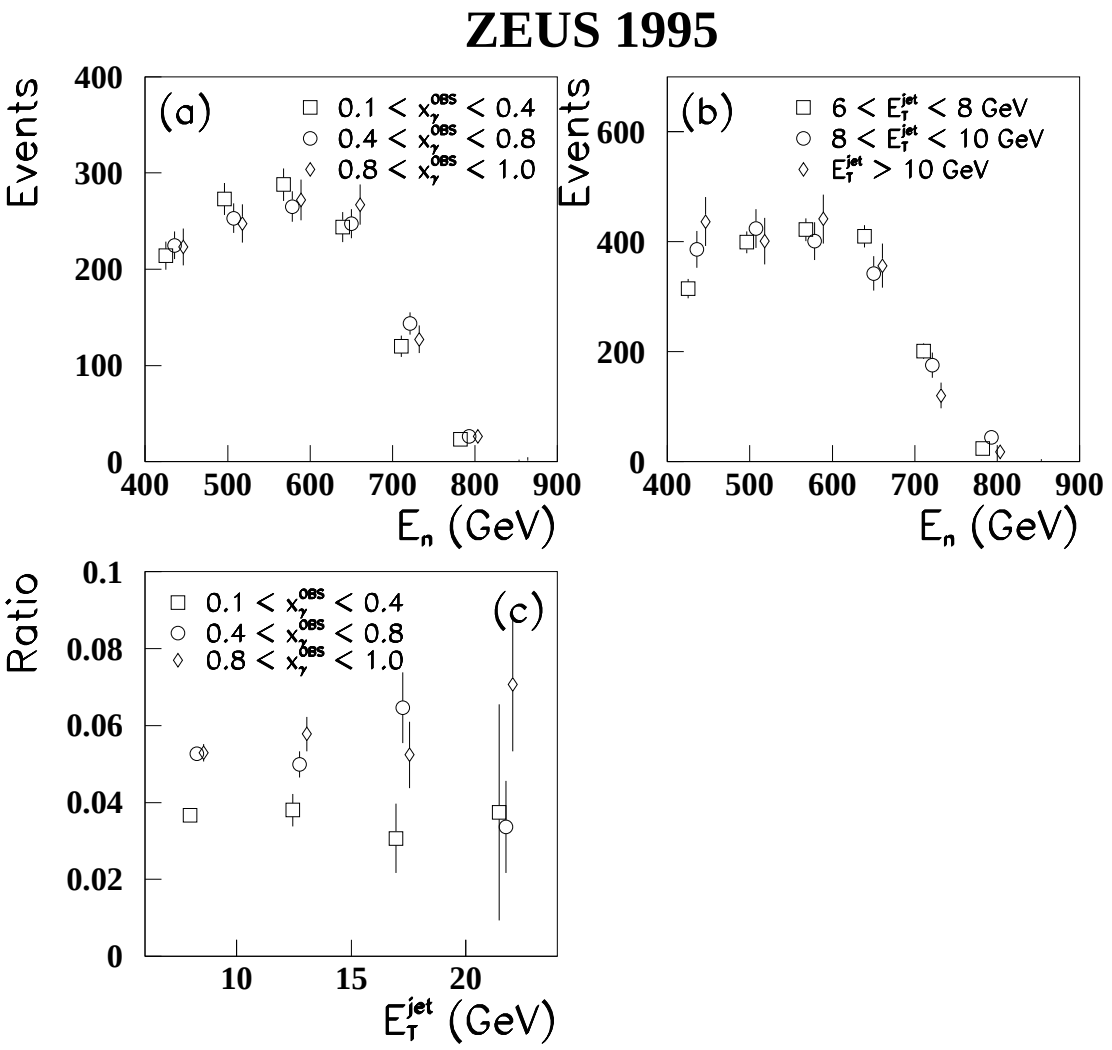

Figure 7: *Uncorrected neutron energy spectra for different ranges of (a) $x_\gamma^{\rm OBS}$ and (b) $E_{\rm T}^{\rm jet}$. The spectra are area-normalized. (c) The ratio of the cross-sections of neutron-tagged to inclusive dijet photoproduction as a function of $E_{\rm T}^{\rm jet}$ for different ranges of $x_\gamma^{\rm OBS}$ (applied to both the inclusive and tagged samples). The points are offset slightly to improve visibility. Only statistical errors are shown. There is an overall normalization uncertainty (not shown) of 9% for (c).*

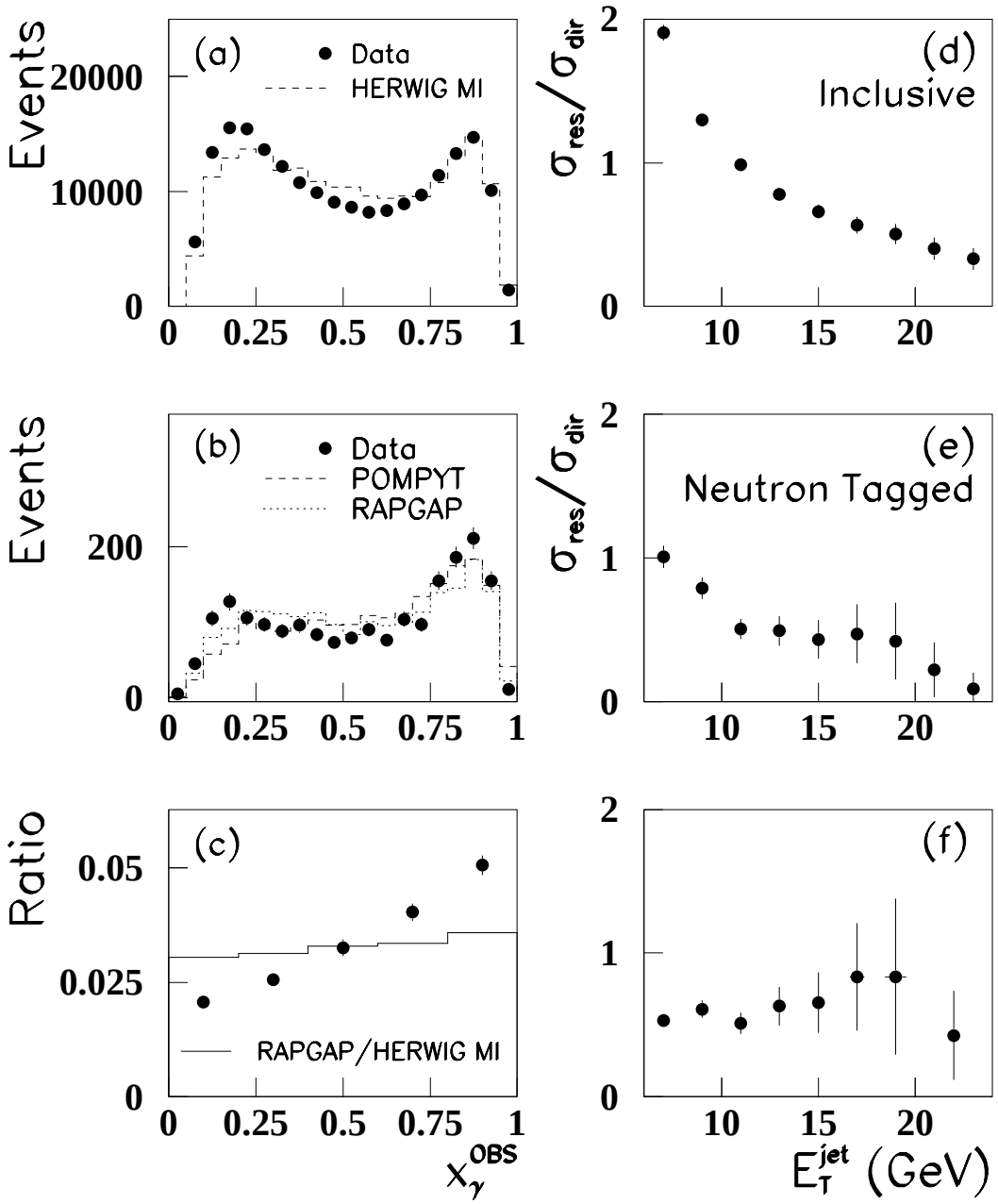

Figure 8: *The uncorrected $x_\gamma^{\rm OBS}$ distribution for (a) inclusive events compared to the expectations of HERWIG with multiple interactions, and (b) for neutron-tagged events compared to the expectations of POMPYT and RAPGAP. The ratio of the neutron-tagged to inclusive $x_\gamma^{\rm OBS}$ distributions is shown in (c) together with the ratio of RAPGAP to HERWIG MI. The Monte Carlo predictions are area normalized to the data in (a,b) and normalized at $x_\gamma^{\rm OBS} = 0.5$ in (c). The ratio of the resolved to direct cross sections as a function of $E_{\rm T}^{\rm jet}$ is shown in (d) and (e) for inclusive and neutron-tagged photoproduction, respectively. Resolved (direct events) are defined by $x_\gamma^{\rm OBS} < 0.75$ ($x_\gamma^{\rm OBS} > 0.75$). The ratio of the ratios shown in (d) and (e), i.e.* [(e)/(d)]*, is shown in (f). Only statistical errors are shown.*

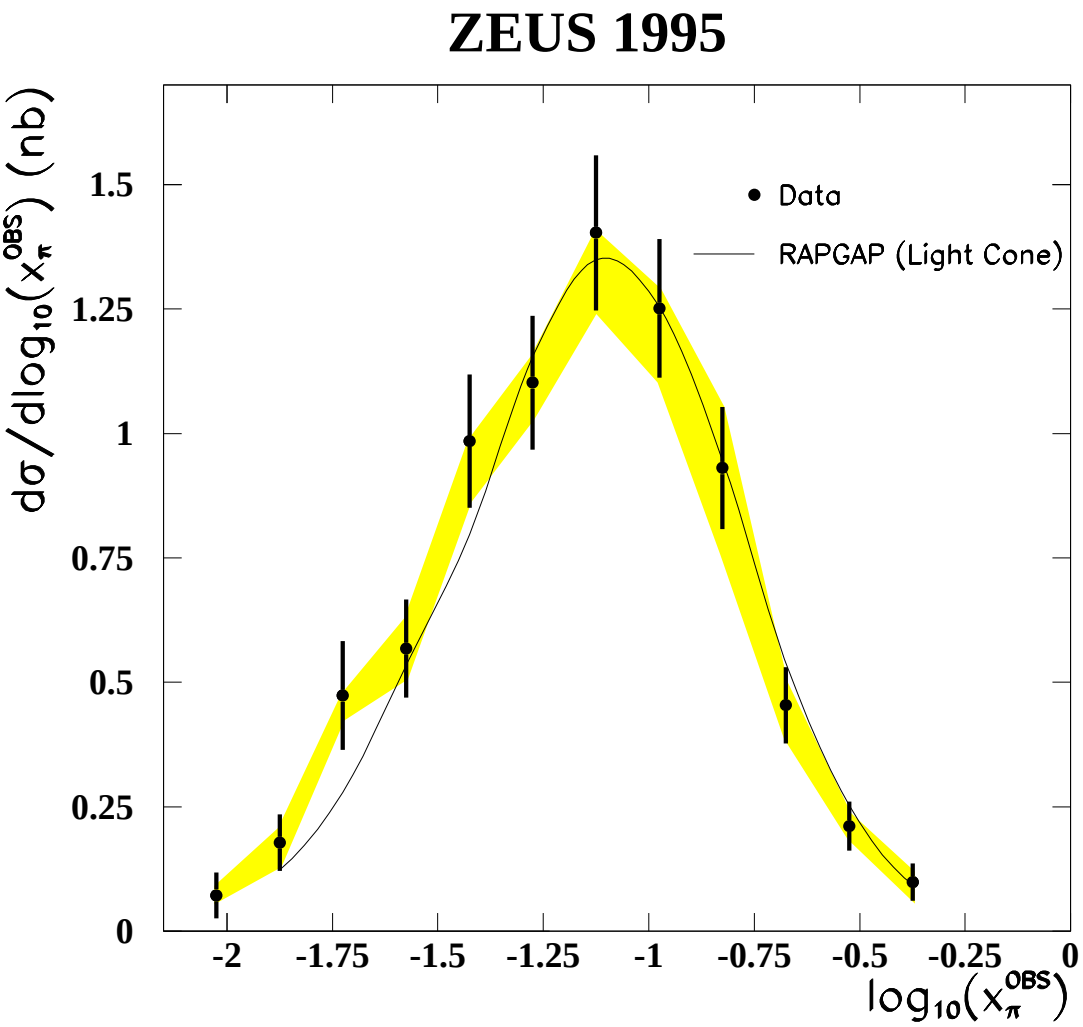

Figure 9: *Differential cross section as a function of $x_\pi^{\rm OBS}$, the fraction of the exchanged pion's momentum participating in the production of the dijet system for the neutron-tagged sample. The measured cross section is compared to the prediction of the Monte Carlo model RAPGAP using the light-cone pion form-factor and the SMRS-P3 pion parton densities. The bands show the systematic uncertainty due to the calorimeter energy scale. The error bars show the statistical error added in quadrature with the remaining systematic error. There is an additional normalization error of 9% which is not shown.*